ELSEVIER

Journal of Materials Processing Technology 186 (2007) 163–173

Journal of Materials Processing Technology

www.elsevier.com/locate/jmatprotec

Analytical relations between hardness and strain for cold formed parts

Fazil O. Sonmez*, Ahmet Demir

Department of Mechanical Engineering, Bogazici University, Istanbul, Bebek 34342, Turkey

Received 13 October 2005; accepted 14 December 2006

Abstract

Our objective in this study is to establish an analytical relation between hardness and effective strain induced in a metal during cold working. In this way, its hardness can be determined from numerically obtained plastic strains without producing the part and taking measurements. For each of the two most commonly used measures of indentation hardness, Vickers' and Brinell's, a separate analytical relation was proposed relying on the previous empirical and numerical studies. The results of the analytical models compared well with the data obtained from the experiments that we conducted. The models were also verified by comparing its predictions with the experimentally determined hardness values reported by previous researchers. The results showed that both of the analytical models can reliably be used to determine hardness distribution within a cold formed part.

Keywords: Brinell hardness; Vickers hardness; Flow curve; Effective strain; Cold forming; Steels

1. Introduction

If a piece of metal is cold formed, the resulting plastic strain distribution will not be uniform because of uneven deformation. Knowing that inducing plastic deformation alters material's strength, different regions of a cold formed part will have different strengths. In order to ensure reliable use of the part, we need to characterize and determine its strength. A practical way of characterizing strength is hardness.

Hardness as a measure of material's resistance to permanent deformation, and thus to wear, is an important quality parameter for the finished product. It is also a measure of forgeability of a material undergoing a cold forming process. Generally, cold formed parts are forged in a number of stages and in each stage the material undergoes additional permanent deformation. The material, during the processing, sometimes becomes so hard that further forming becomes impossible without fracturing the part. In order to continue the process, it should be heat treated, and thus its hardness should be reduced. Therefore, it is crucial to know whether all stages can be achieved consecutively without any interruption of forming process or a heat treatment is necessary at some intermediate stage.

Because of being an important quality criterion and a means of determining formability of the material, we need to determine the hardness of a part. Trial and error, by producing prototypes, taking measurements and repeating the process, is not a feasible approach. It is difficult, time consuming, and costly. Estimating the hardness distribution without actually making the part is a more desirable approach. In this way, we may judge the suitability of the material for the chosen processing, or predict whether the end product will have the desired hardness levels or require a final heat treatment, or we may decide whether the process can be completed in one stage, or in successive stages with intermediary heat treatments reducing the hardness to provide forgeability.

Brinell and Vickers hardness criteria are two of the most commonly used standards for characterizing materials hardness. Hence, many researchers focused their effort on finding a relation between these standard hardness criteria and effective strain. Kim et al. [1] performed an upsetting experiment, and then measured the hardness at various locations in the part. They also calculated effective strain distribution in the upset part through a FE analysis of the upsetting process. By correlating the measured hardness and the numerically found strains, they found a relation between Vickers hardness and effective strain. They also checked the validity of this relation by comparing numerically determined effective strain distribution in a backward extruded can to the measured hardness distribution. Gouveia et al. [2,3] performed a similar study for cold forward extrusion. They obtained a relation between Vickers hardness and effective strain by measuring the hardness at the center of cylindrical specimens compressed at specific ratios. According to the

* Corresponding author. Tel.: +90 212 359 7196; fax: +90 212 287 2456.
E-mail address: sonmezfa@boun.edu.tr (F.O. Sonmez).

0924-0136/$ – see front matter © 2007 Elsevier B.V. All rights reserved.
doi:10.1016/j.jmatprotec.2006.12.031

compression ratio, the compressed specimens had known values of effective strain. They used their relation to verify the numerically calculated effective strain distribution in an extruded part by comparing with the measured hardness distribution. Petruska and Janicek [4] also conducted a similar study. They carried out compression and extrusion tests on steel and copper specimens. After cutting the specimens through their symmetry axes, they measured hardness at various points. By relating the measured values of Brinell or Vickers hardness to numerically obtained strains, they obtained empirical equations. Ruminski et al. [5] obtained an empirical relation between Vickers hardness and effective strain to determine the mechanical property distribution in cold drawn tubes. However, all of these were empirical relations specific to certain materials with a certain flow curve. If one seeks a relation between hardness and strain for another material, an upsetting test, hardness measurements, and FE simulations are required followed by correlation with results. Choi et al. [6] avoided this burdensome procedure by performing a FE simulation of the Brinell hardness test for a cold formed material. They numerically obtained Brinell hardness of a material that has undergone a certain extent of plastic strain. Based on the calculated hardness they found a relation between hardness and strain, and then verified this relation by comparing the predicted hardness distribution with the measured values. Although they avoided the cumbersome experimental work that the previous methods required, their approach still poses difficulties concerning accurate FE modeling of a Brinell indentation, and computational expense of such a nonlinear contact problem with moving contact boundaries. Besides, the obtained relation is not general, but particular to the material under concern. Similarly, Tekkaya [7] carried out a FE analysis of conical indentation on a cold worked part to find the equivalent pyramidal Vickers hardness and obtained a relation between Vickers hardness and flow stress.

In this study, we propose an analytical relation between the Brinell hardness of a cold formed material and the effective strain based on the flow curve constants of the unformed material. We also examine the applicability of a previously proposed relation for Vickers hardness and yield stress to this purpose. In this way, formidable experimental and numerical procedures can be avoided.

2. Approach to the problem

The Brinell hardness test (Fig. 1) is performed by forcing a hardened steel (or tungsten carbide) ball with diameter D onto the part being tested with a specified force, F, and measuring, by a magnifier or microscope, the diameter of the indented area, d. The Brinell hardness, H_B, is defined as the load per unit surface area of the permanent impression:

$$H_B = \frac{F/D^2}{(\pi/2)\left(1-\sqrt{1-(d/D)^2}\right)} \quad (1)$$

Here, F is in kgf, D and d are in mm. Accordingly, the unit of H_B is kgf/mm^2. For steels having hardness less than $650H_B$,

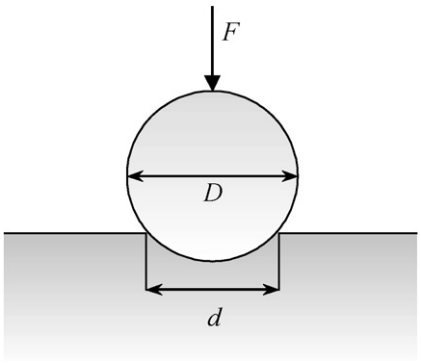

Fig. 1. A schematic for the spherical indentation of the Brinell hardness test.

the standard value of the F/D^2 ratio is 30 kgf/mm^2. Usually, the chosen values for F and D are 3000 kgf and 10 mm [8]. Hence, having measured or estimated the indentation diameter, d, one may easily calculate H_B.

Vickers hardness test shares the same procedure except that a pyramidal indenter is used. It (Fig. 2) is performed by forcing a diamond square pyramid onto the part being tested and measuring the diagonals of the indented area, s. The Vickers hardness, H_V, is defined as the load divided by the surface area of the permanent impression. The angle between the opposite faces of the pyramid is 136° such that the base of the pyramid has an area equal to 0.9272 times its lateral area [9]. Thus, Vickers hardness is given by

$$H_V = 0.9272 P_m \quad (2)$$

where P_m is the mean pressure (force divided by the projected area), thus

$$H_V = 0.9272\left(\frac{2F}{s^2}\right) \quad (3)$$

The unit of H_V is also kgf/mm^2. Once the diagonal of the indentation, s, is measured, or predicted through a model, Vickers hardness can be calculated.

We may assume that the deformation behavior of the material fits a simple power law such that if the material is under uniaxial loading, the true stress-true strain curve can be described by

$$\sigma = \kappa\varepsilon^n \quad (4)$$

where κ and n are material constants. The strain hardening exponent, n, ranges from 0.0 (zero work hardening) to an upper limit of about 0.5 [10]. In this study, analytical equations were

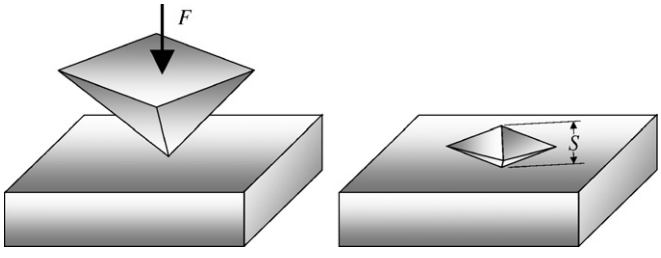

Fig. 2. Schematic for the pyramidal indentation of Vickers hardness test.

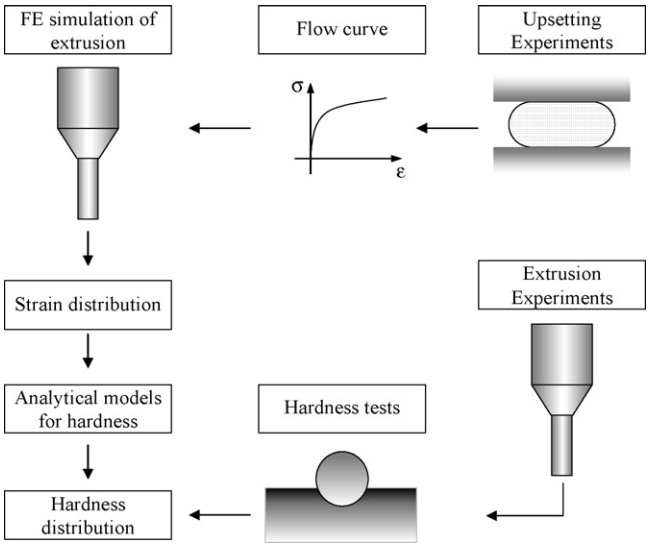

Fig. 3. Schematic of the procedure for verifying the analytical model.

proposed that relate the diameter, d, of a Brinell's spherical indentation, and the diagonal, s, of a Vickers' pyramidal indentation to effective strain and flow curve constants κ and n so that hardness of cold formed parts can be predicted.

Fig. 3 describes the procedure that we followed to verify the analytical models. First, two different materials were selected and their flow curves were determined through upsetting (compression) experiments. Effective strain at the central line of the extruded parts away from the edges was already known analytically. Besides, FE analysis of the extrusion process was carried out to find the effective strain distribution. Thus, it was possible to ascertain the region where analytically calculated strains were valid. Then, the hardness corresponding to the effective strains was predicted through the analytical models. The results were then compared with the measured hardness. The analytical models were also verified by checking how well it predicts the experimental results reported by previous researchers.

3. The analytical model to predict Brinell hardness

The mechanical behavior of an indented solid can be characterized as purely elastic, elasto-plastic, or fully plastic. If the indentation force is small, the material elastically deforms and upon unloading the surface recovers to its original shape. A further increase in the load leads to plastic deformation; then plastic region extends, during which resistance of the material against deformation increases due to work hardening. Continued indentation thus requires larger and larger mean pressure. Beyond the elastic–plastic regime, a fully plastic regime follows, in which plastic zone extends over the whole region around the indentation. Hardness measurements are carried out in the fully plastic regime; hence correlation of experimental and analytical results should be made in this regime.

In 1908 Meyer developed an empirical relation [9] such that the ratio of indentation diameter to the ball diameter, d/D, increased with the mean pressure, P_m, as

$$P_m = k\left(\frac{d}{D}\right)^m \tag{5}$$

where P_m is the load per unit projected area

$$P_m = \frac{F}{\pi d^2/4} \tag{6}$$

The data provided by O'Neill in 1944 [9,11] suggested that the power m in Eq. (5) was about equal to the strain hardening exponent, n, in Eq. (4). Further experimental studies confirmed this finding [12,13].

Based on indentation tests performed on highly worked materials Tabor [10,11] found that mean pressure, P_m, was about equal to $3\sigma_e$, flow stress, in the fully plastic regime regardless of the indentation size. Because they were incapable of further appreciable work hardening, they can be considered to be ideally plastic material. Accordingly, flow stress, σ_e, can be assumed to be uniform around the indented region. On the other hand, when a work hardening material is indented by a spherical indenter, the flow stress (or yield stress, S_y) increases in the indented region as a result of the strain hardening of the material. We should recognize that the extent of deformation, or strain (ε), changes from one point to another in the indented region, so does the flow (or yield) stress according to Eq. (4). This means that for work hardening materials, flow stress not only varies with deeper penetration but also varies spatially in the indented region. Tabor [11] assumed that at a material point developed a flow stress, σ_e, that could be considered to be representative of the overall deformation. He further assumed that the representative stress had a linear relation with the average pressure.

$$P_m = \alpha\sigma_e \tag{7}$$

where α is a constant, called "constraint factor." At this material point, the representative stress, σ_e, and strain, ε_e, are also related according to Eq. (4).

$$\sigma_e = \kappa\varepsilon_e^n \tag{8}$$

Tabor, reasoning from the equality of strain distributions for indentations at which d/D ratio is the same, because of the same deformed shape, concluded that the representative strain would also depend on this ratio. In order to find the point of representative flow stress, Tabor first established an empirical relation between pyramidal Vickers hardness and the flow stress of the material based on measured values of hardness on specimens compressed by specific ratios, therefore with known flow stress. Then, he conducted micro-pyramidal indentations on the surface of spherical Brinell indentations, and thus determined the flow stress of the deformed material at various locations on the free surface. Based on the data, he found out that the flow stress at the edge of the indentation was proportional the mean pressure, P_m, over a wide range of indentation sizes (d/D) such that Eq. (7) holds with a value of α approximately equal to 2.8 (for various materials, it was between 2.6 and 3.0). Accordingly, he supposed that it might be used as a

representative value for the overall deformation of the material around the impression. The corresponding representative strain at the edge found from Eq. (8) turned out to be linearly related to the d/D ratio (confirming Eq. (5) and equality of n and m) as

$$\varepsilon_e = \beta \frac{d}{D} \tag{9}$$

Here, β was about equal to 0.2 independent of n or κ. Substituting Eqs. (6), (8) and (9) into Eq. (7), we obtain

$$\frac{F}{\pi d^2/4} = \alpha\kappa \left(\beta \frac{d}{D}\right)^n \tag{10}$$

Here left hand side represents the mean pressure, P_m, which takes the same value as long as d/D remains the same as the experiments demonstrate. The ratio of mean pressure P_m, to yield stress S_y (or σ_e), at the onset of permanent deformation during indentation takes a value of about 1.1 [14–16]. In order to induce a deeper indentation, this ratio needs to be increased, but when the ratio becomes equal to α (in Eq. (7)) in the fully plastic regime, in which hardness measurements are taken, it remains constant [11]. Taking out the indentation diameter, d, in Eq. (10), we get

$$d = \left(\frac{4FD^n}{\pi\alpha\kappa\beta^n}\right)^{1/n+2} \tag{11}$$

Substituting for d in Eq. (1), and rearranging, we may express the Brinell hardness, H_B, in terms of the known properties.

$$H_B = \frac{F/D^2}{(\pi/2)\left(1 - \sqrt{1 - ((4/\pi\alpha\kappa\beta^n)(F/D^2))^{2/n+2}}\right)} \tag{12}$$

Eq. (12) implies that as long as the F/D^2 ratio remains constant (the standard is 30 kgf/mm^2 for steels), the same Brinell hardness is obtained for a given material regardless of the applied force, F. This equation, of course, is valid only in the fully plastic regime. Having determined flow curve constants (κ and n), we can easily calculate the Brinell hardness.

In a cold forging process, plastic strains are induced, and consequently hardness of the work-piece increases due to strain hardening. Eq. (12), however, does not account for the effect of work hardening. Therefore, it is valid only for materials with no prior deformation. Tabor confirmed that initial uniaxial strain, ε_0, is additive to the representative strain, ε_e. Eq. (9) then becomes

$$\varepsilon_e = \varepsilon_0 + \beta \frac{d}{D} \tag{13}$$

Substituting Eqs. (6), (8) and (13) into Eq. (7), we may express the average pressure as

$$\frac{F}{\pi d^2/4} = \alpha\kappa \left(\varepsilon_0 + \beta \frac{d}{D}\right)^n \tag{14}$$

Eq. (14) may not be solved for d analytically. We need to employ numerical methods. After substituting the numerically obtained value for d in Eq. (1), we may easily calculate H_B. Nevertheless, Eq. (14) is valid for uniaxially loaded and deformed parts. Its validity for multiaxially loaded and deformed parts is investigated in this study.

3.1. Effective strain

During forging of intricate parts, unlike uniaxial loading, deformation state becomes very complex. At a material point, all of the strain components, ε_{ij}, may be nonzero. However, in order to be able to employ Eq. (13) we need a single strain, ε_0, that is representative of the prior deformation at that point.

Considering the strain components, ε_{ij} as a superposition of elastic and plastic components, ε^e_{ij} and ε^p_{ij}, we may express ε_{ij} as

$$\varepsilon_{ij} = \varepsilon^e_{ij} + \varepsilon^p_{ij} \tag{15}$$

Plastic deformation induced during forging is so extensive that elastic deformation can be assumed to be negligible, thus

$$\varepsilon_{ij} \cong \varepsilon^p_{ij} \tag{16}$$

One may define deviatoric strains, e_{ij}, as

$$e_{ij} = \varepsilon_{ij} - \frac{1}{3}\varepsilon_{kk}\delta_{ij} \tag{17}$$

where ε_{kk} is the sum of the normal strains, $\varepsilon_{11} + \varepsilon_{22} + \varepsilon_{33}$, which represents dilatation (or volume change per unit volume), and $\delta_{ij} = 1$ for $i = j$, $\delta_{ij} = 0$ for $i \neq j$. According to the deformation theory of plasticity, plastic strain involves only a change in shape, but no change in volume ($\varepsilon_{kk} = 0$). Thus, the stain components can be expressed as

$$\varepsilon_{ij} \cong e_{ij} = \begin{bmatrix} \frac{1}{3}(2\varepsilon_{11} - \varepsilon_{22} - \varepsilon_{33}) & \varepsilon_{12} & \varepsilon_{13} \\ \varepsilon_{12} & \frac{1}{3}(2\varepsilon_{22} - \varepsilon_{11} - \varepsilon_{33}) & \varepsilon_{23} \\ \varepsilon_{13} & \varepsilon_{23} & \frac{1}{3}(2\varepsilon_{33} - \varepsilon_{11} - \varepsilon_{22}) \end{bmatrix} \tag{18}$$

Effective strain is defined as

$$\varepsilon_0 = \sqrt{\frac{2}{3} e_{ij} e_{ij}} \tag{19}$$

In expanded form

$$\varepsilon_0 = \sqrt{\frac{2}{3}(e^2_{11} + e^2_{22} + e^2_{33} + 2e^2_{12} + 2e^2_{13} + 2e^2_{23})} \tag{20}$$

As can be seen, in uniaxial loading of an incompressible material ($\nu = 1/2$), where only σ_{11} is nonzero, effective strain

reduces to ε_{11}. For further information, one may refer to books on plasticity like Ref. [17].

In this study, we assume that Eq. (13) as well as Eq. (14) are valid for multiaxial strain state if effective strain is used for ε_0. Ruminski et al. [5] found that compression and tension specimens deformed to the same level of effective strain possessed about the same hardness for the materials they tested. This fact supports our assumption made in deriving Eq. (14) that hardness of a material is uniquely related to the level of effective strain regardless of the deformation history. However, for materials for which tension and compression flow curves are highly discrepant such as austenitic stainless steels [7], or steels having untempered martensitic structure [18] validity of Eq. (14) will be questionable.

3.2. The factors α and β

Tabor [11] experimentally determined the values of α and β in Eq. (10) as 2.8 and 0.2. Researches investigated through empirical, theoretical and numerical studies whether these values were just empirical fit obtained by just averaging the data on a few chosen materials, or they possessed a general validity. Most of these researchers confirmed the form of Eq. (10), but differed on their choice of appropriate values for α and β [16,19–21]. FE analyses of some researchers [15,22–25] confirmed Tabor's findings. Some others [12,13,26–29] proposed different relations between mean pressure, P_m, and indentation diameter, d.

Ahn and Kwon [30] conducted instrumented spherical indentation tests on steel specimens and determined the contact diameters from the measured load–depth curves. They found the ratio of mean pressure to representative stress, P_m/σ_e, to be constant in the fully plastic regime and equal to 3.0 independent of strain hardening exponent, n. σ_e is the stress corresponding to the representative strain, ε_e. They advocated a form for representative strain, which was different from Eq. (9), given as

$$\varepsilon_e = \beta \frac{1}{\sqrt{1-(d/D)^2}} \frac{d}{D} \tag{21}$$

where β is a constant. A value of 0.1 provided the best agreement between the experimental results and the equation. One should note that if $(d/D)^2$ is negligibly small, Eq. (21) approximates Eq. (9).

Matthews [21] developed a model for spherical indentation process by generalizing the linear formulation for contact pressure between spheres to nonlinear deformation of work hardening materials during indentation. His model conforms to Tabor's equation, but here α depends on strain hardening exponent, n.

$$\alpha = \frac{6}{2+n}\left(\frac{40}{9\pi}\right)^n \tag{22}$$

FE analysis of spherical indentation carried out by Taljat et al. [28] also showed dependence of α on strain hardening exponent n.

Review of the literature reveals that there are disagreements among researchers regarding the relation between mean pressure and the extent of indentation. Reliability of the proposed relations should to be determined based on empirical data.

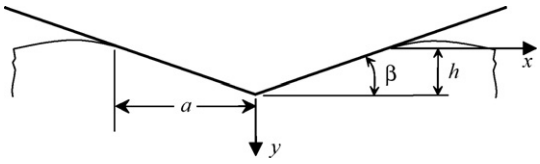

Fig. 4. Geometry of a pyramidal indentation.

4. The analytical model to predict Vickers hardness

In a Vickers hardness test, because a pyramidal indenter is used, only the size of the impression changes with the applied force, while its shape remains the same, i.e. the ratio of the indentation depth to contact length, h/a, remains constant as the indentation depth, h, is increased (Fig. 4). Accordingly, normalized strain state can also be assumed to be independent of the indentation size as long as it is insignificantly small in comparison to the size of the part. That means $\varepsilon(x/a, y/a)$ is the same independent of indentation size. Then the corresponding normalized stress state should also be the same. The indentation pressure, P_m, generating the stress state may also be assumed to be independent of the extent of the indentation. Vickers hardness, accordingly, is independent of the size of the indentation, and therefore of the load [9] as long as it is larger than 500 gf [8]. Smaller loads may not give accurate results due to surface irregularity and material inhomogeneity. On the other hand, a standard force should be applied on the spherical indenter of the Brinell hardness test for consistent readings.

Tabor [11] assumed that there is again a representative flow stress, σ_e, that is linearly related to mean pressure:

$$P_m = c'\sigma_e \tag{23}$$

where c' is a constant. Considering that the strain state is independent of the size, the representative yield strain, ε_e, corresponding to σ_e is constant and independent of the load and hardness. Tabor [11] empirically determined its value as about 0.08, and observed that corresponding σ_e, obtained from stress–strain curve of the material, is linearly related to Vickers hardness, and also that the proportionality constant c' relating the mean pressure, P_m, to σ_e was about equal to 3.2. From Eqs. (2), (23) and (8), the following equation is obtained for the relation between Vickers hardness and flow constants:

$$H_V = c\kappa(\varepsilon_e)^n \tag{24}$$

Here, the values of c and ε_e are 2.9 ($\approx 0.9272 \times 3.2$) and 0.08, respectively. Based on the hardness measurements made on a material that had been compressed by various amounts, Tabor concluded that the initial uniaxial strain, ε_0, is additive to the representative strain, ε_e. H_V may then be expressed that

$$H_V = c\kappa(\varepsilon_0 + \varepsilon_e)^n \tag{25}$$

However, applicability of this equation to multiaxially deformed materials has not been investigated.

Tekkaya [7] assumed the form of Eq. (24) to be valid and proposed a value of 2.475 for the constraint factor, c, and 0.112 for plastic strain based on a FE analysis of conical indentation and experiments conducted on five different steels with four different extrusion ratios. Larsson [31] carried out a FE analysis of Vickers indentation and found the representative strain approach of Tabor valid in the fully plastic regime. The numerical results fitted to Eq. (24) with $c = 2.6$ and $\varepsilon_e = 0.15$. Jayaraman et al. [32] based on a FE analysis of cone indentation proposed an equation similar in form to Eq. (24), but depending on elastic modulus, E.

$$\frac{P_m}{E} = 1.34\left(\frac{\sigma_e}{E}\right)^{0.84} \tag{26}$$

Here, equivalent stress, σ_e, is calculated at 7% plastic strain.

Johnson [33], inspired by Marsh's study [34], who found a correspondence between the pyramidal indentation pressure and the pressure found by Hill [35] necessary to expand a spherical cavity from zero radius in an elastic perfectly plastic solid, assumed that displacements produced by any blunt indenter (having small β) were nearly radial from the point of first contact and plastic strain contours were hemispherical in shape. He considered the contact surface of a conical indenter being embedded in a hemispherical core of radius a. This core replaced the cavity in the theoretical model developed by Hill [35]. A hydrostatic uniform stress, p, was assumed to exist within the core $(r \leq a)$ equal in magnitude to the applied pressure. The stress and strain states outside the core $(r > a)$ were taken to be the same as predicted by Hill's model. Imposing compatibility between the radial displacement at the core boundary $(r = a)$ and the volume of material displaced by the indenter, the pressure within the core was found to be

$$\frac{P}{\sigma_e} = \frac{2}{3}\left[1 + \ln\left(\frac{E}{3\sigma_e}\tan\beta\right)\right] \tag{27}$$

where β is the inclination angle as shown in Fig. 4. Eq. (27) is rigorously valid only for elastic–perfectly plastic materials σ_e is then taken to be equal to the yield strength, S_y. If this equation is used for strain hardening materials, σ_e is the stress corresponding to the representative strain, ε_e, which is equal to $0.2\tan\beta$, where for pyramidal indentation $\beta = 19.7^\circ$, for which a cone replaces the same volume of material as a Vickers pyramid. Eq. (27) is valid in the elastic–plastic regime, where $(E/\sigma_e)\tan\beta$ takes a value between 2 and 50. In the fully plastic regime, core pressure becomes equal to $2.8\sigma_e$ and then remains constant.

Studman et al. [36] introduced a correction to Johnson's model by taking the core as a region where stresses change from purely hydrostatic just under the indenter to values which satisfy the Von Mises yield criterion at the core boundary, yielding

$$\frac{P}{\sigma_e} = 0.5 + \frac{2}{3}\left[1 + \ln\left(\frac{E}{3\sigma_e}\tan\beta\right)\right] \tag{28}$$

Giannakopoulos et al. [37] based on a finite element analysis of Vickers indentation found the form of Eq. (27) valid for linearly strain hardening materials in the elastic–plastic regime. Only, the representative strain, ε_e, was much higher, 0.3, and the factor was 0.27 instead of 2/3.

Mata et al. [38], assuming the form of Eq. (27) to be valid also for strain-hardening materials, carried out a finite element analysis of the indentation process and determined the constants of Johnson's model to determine hardness of power-law hardening materials. They considered a rigid conical indenter with an inclination angle, β, of 19.7°, which they assumed to be also applicable to Vickers pyramidal indentation. Correlation of the numerical results and the model gave

$$\frac{P_m}{\sigma_e} = 1.440 + 0.264\ln\left(\frac{E}{\sigma_e}\right) \tag{29}$$

where P_m is the mean pressure. They also found Tabor's equation, Eq. (24), to be rigorously valid for elastic power-law-strain hardening solids deformed in the fully plastic regime, but for different values of $c = 2.7$ and $\varepsilon_e = 0.10$. Mata and Alcala [39] obtained an equation that was valid for both elastic–plastic and fully plastic regimes by fitting a function to the FE numerical results.

$$\frac{P_m}{\sigma_e} = -0.0023\left[\ln\left(\frac{E}{\sigma_e}\right)\right]^4 + 0.0647\left[\ln\left(\frac{E}{\sigma_e}\right)\right]^3 - 0.6817\left[\ln\left(\frac{E}{\sigma_e}\right)\right]^2 + 3.1968\left[\ln\left(\frac{E}{\sigma_e}\right)\right] - 2.9261 \tag{30}$$

Here, representative stress, σ_e, is the stress that corresponds to a strain of 0.1. Eq. (30) is valid for materials having strain hardening exponents, n, between 0.1 and 0.4. Later, Mata and Alcala [40] developed a procedure to include the effect of friction on indentation.

Cheng et al. [41–43] performed a finite element analysis of indentation by a rigid cone and calculated the indentation depth as a function of applied load. Through a dimensional analysis, they found Tabor's representative strain approach to be valid, but for a value of $\varepsilon_e = 0.1$. The numerical results showed that the ratio of mean pressure to representative stress, P_m/σ_e, was independent of strain hardening exponent, n. However, this ratio depended on the ratio of yield stress to elastic modulus, S_y/E, decreasing with increasing S_y/E. The value of P_m/σ_e was 2.8, when S_y/E approached to zero, which is the case for steels. One should note that mean pressure, P_m, was defined in this study as the load divided by projected area of indentation under load. As shown in another study [44], the mean pressure calculated based on this definition may be quite different from the mean pressure based on the residual projected area after unloading, based on which Vickers hardness is defined.

Bolshakov and Pharr [45] carried out a FE analysis of axisymmetric conical indentation, and found Tabor's equation to be valid, but at 10% strain and for materials with small values of σ_e/E.

Dao et al. [46] and Chollacoop et al. [47] carried out a large deformation finite element analysis of Vickers indentation and correlated elasto-plastic properties of materials with their indentation response through a dimensional analysis. Representative plastic strain turned out to be 0.033, i.e. $\varepsilon_e = S_y/E + 0.033$. By fitting a number of dimensionless functions to numerical data, they obtained a relation between mean pressure, P_m, and elasto-

plastic properties (E, n, κ). A similar study conducted by Bucaille et al. [48] confirmed these findings. Casals and Alcala [49] also found dimensionless functions relating hardness to E, n, and σ_e.

5. Comparison between measured and predicted values of hardness

In order to test the suitability of the models, a comparison is made between the measured hardness of materials with known flow properties and the hardness predicted by these analytical models. Because we focused on forging of steels in this study, we only considered steel properties reported in the literature. As seen in Table 1, the flow parameters (κ and n) and hardness of the 37 chosen materials have a wide range of values (0.04–0.264 for n, 540–2834 MPa for κ, 92–642 kgf/mm^2 for H_B). Because the hardness of these materials was measured before any prior deformation (i.e. work hardening), Eq. (12) was employed for Brinell hardness using the suggested α and β values. The empirical values ($\alpha = 2.8$, and $\beta = 0.2$) proposed by Tabor [11], and confirmed by the analyses of Hill et al. [25] and Follansbee et al. [15,22] turned out to be the most appropriate ones in predicting the hardness of a steel material. The average error in H_B predicted by Eq. (12) for the chosen materials is 5.6% with a standard deviation of 4.3, and the maximum error is 15.2%. There is no need to decrease the value of α for low strength steels in contrast to the suggestion made by Tirupataiah and Sundararajan [12] for lower strength materials such as iron and copper. As for the models developed for pyramidal indentation, again the equation, Eq. (24), proposed by Tabor turned out to give the best correlation with measured Vickers hardness. The average error in H_V predicted by Eq. (24) is 5.6% with a standard deviation of 4.6, and the maximum error is 18%.

Because our objective is to estimate Brinell or Vickers hardness of cold forged products, the validity of the models in

Table 1
Measured hardness and the percentage error in calculated hardness (Eqs. (12) and (24)) of materials with no initial strain

Material (steel)	κ (MPa)	n	Measured hardness, H_V	%error in predicted H_V (Eq. (24))	%error in predicted H_V[a] (Eq. (12))
Low carbon steel, 0.077C [50]	593	0.25	92[b]	3.8	2.8
Low carbon steel, 0.065C [50]	540	0.17	99[b]	1.4	5
AISI 1010 [1]	665	0.255	103	0.5	1.6
WNr. 1.0303 [2,3]	685.2	0.185	115	10.3	8.9
XC18 [51]	664	0.10	149	2.4	−1.0
SCM415 [6]	768	0.139	150[a]	6.6	3.9
Z2CN18-10 [51]	862	0.21	155	−3.2	−4.1
Mild steel [11]	1000	0.249	156	1.1	0.8
XC80 [51]	921	0.17	167	6.2	4.0
0.46%C steel [52]	1180[c]	0.264[c]	171	4.8	4.2
AISI 4130 annealed [53]	888	0.145	173[a]	2.6	5.2
35CD4 [51]	819	0.09	194	−0.5	−3.5
AISI 316L austenitic stainless steel [54]	1760	0.4	194	−2.3	−2.0
Annealed low alloy steel 0.34C, 1.2Cr [18]	925[c]	0.16[c]	202	−9.6	−11.3
XC48 [51]	1133	0.16	205	9.1	6.1
16NC6 [51]	1026	0.17	206	−4.1	−6.4
100C6 [51]	1023	0.14	206	3.1	0.6
42CD4 [51]	939	0.10	214	0.8	−2.0
Z38CDV5 [51]	1136	0.17	223	−1.9	−4.4
XC38 [51]	1102	0.11	232	6.4	3.7
XC65 [51]	1607	0.24	232	11.7	7.6
AISI 329 dublex stainless steel [54]	1062	0.17	235	−13.0	−15.0
AISI 4130 annealed [53]	1150	0.07	242[a]	14.7	15.2
0.3C, 0.4Mo, 1.4Mo,1.6Ni temperature at 725 °C [12]	1137	0.120	260	−4.5	−7.0
ASTM A514, T1 [55]	1103	0.088	269[a]	−3.1	−6.4
A508B [56]	1133	0.105	272	−5.6	−8.7
SAF 2507 dublex stainless steel [54]	1307	0.19	275	−13.0	−15.2
35NC15 [51]	1235	0.08	287	4.0	1.4
Z15CN17-03 [51]	1403	0.10	304	6.0	3.3
AISI 4130 tempered at 670 °C [29]	1300	0.096	314	−3.9	−6.5
AISI 4130 tempered at 550 °C [29]	1375	0.070	356	−4.3	−6.8
SAE 4340 steel [57]	1659	0.0749	383	6	3.4
0.3C, 0.4Mo, 1.4Mo, 1.6Ni temperature at 425 °C [12]	1534	0.061	425	−8.5	−10.5
AISI 4130 tempered at 400 °C [29]	1860	0.049	487	−0.2	−1.2
AISI 4130 tempered at 300 °C [29]	2213	0.056	569	−0.2	−1.4
0.3C, 0.4Mo, 1.4Mo, 1.6Ni temperature at 200 °C [12]	2163	0.050	571	−1.3	−2.1
Maraging steel [58]	2838[c]	0.04[c]	642	18.2	14.6

[a] Brinell hardness was converted to Vickers hardness using the conversion table for steels [59].
[b] Rockwell hardness (scale B) was converted to Vickers hardness.
[c] These values were estimated using the curve provided in the paper.

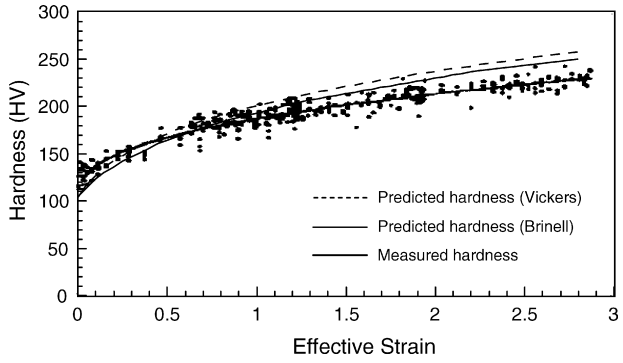

Fig. 5. Data points indicate the measured hardness corresponding to the numerically calculated values of effective strain [1] for AISI 1010. The thicker line shows the empirical curve obtained by curve fitting of the data points. The thinner solid line and dashed line show the hardness predicted by Eq. (14), together with Eq. (1), and Eq. (25), respectively.

estimating the hardness of permanently deformed materials is our concern in this study. Here, we examine whether Eqs. (25) and (14) together with Eq. (1) are also valid in predicting Vickers and Brinell hardness of cold worked parts where deformation behavior is complex if effective strain is used for ε_0 as representative of the prior deformation. We compare the predictions of the proposed equations first with the experimental data reported by Kim et al. [1]. In Fig. 5, data points indicate the hardness measured at specific locations in compression specimens corresponding to the numerically calculated effective strains. The thicker line shows the empirical curve obtained by curve fitting of the data points ($H_V = 102.8 + 84.9\varepsilon_0^{0.4}$) [1]. The thinner solid line shows the Brinell hardness predicted by the proposed equation (Eq. (14) together with Eq. (1)) using the flow parameters of the undeformed material (the Brinell hardness was converted to Vickers hardness using the conversion table in Ref. [59]). The dashed line shows the Vickers hardness predicted by Eq. (25). Calculated values of hardness are almost within the range of the data scatter. Only Vickers hardness predictions are a little out of range for very large effective strains. The empirical values ($\alpha = 2.8$, $\beta = 0.2$ in Eq. (14), and $c = 2.9$, $\varepsilon_e = 0.08$ in Eq. (25)) proposed by Tabor [11] again provided the best fit.

Fig. 6 provides another comparison between the predicted and measured hardness. The triangular marks show the hardness

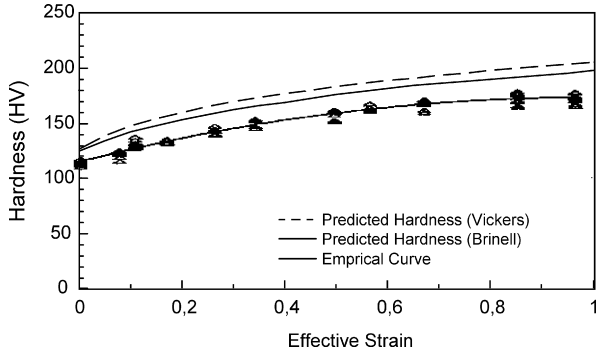

Fig. 6. The thicker line shows the empirical curve obtained by curve fitting of the data points ($H_V = -60.7\varepsilon_0^2 + 119.1\varepsilon_0 + 115.1$) [2]. The thinner solid line and dashed line show the hardness predicted by Eq. (14), together with Eq. (1), and Eq. (25), respectively.

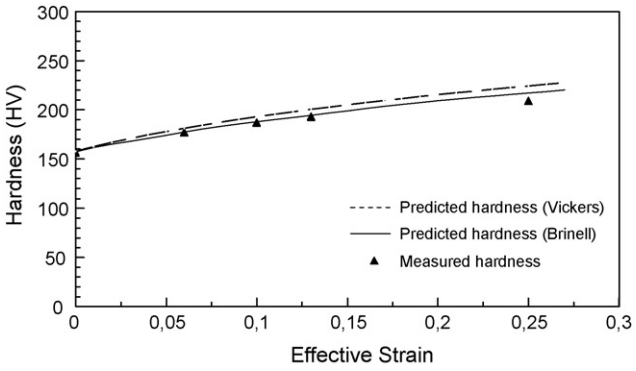

Fig. 7. Data points indicate the measured hardness of a mild steel [11]. The solid line and dashed line show the hardness predicted by Eq. (14), together with Eq. (1), and Eq. (25), respectively.

measured by Gouveia et al. [2,3] at the center of cylindrical specimens compressed at specific ratios, therefore with known values of effective strain. Although, the analytical models somewhat overestimate the hardness, the predicted trend in hardness with induced deformation agrees with the experimentally determined trend. The maximum error is 14% and 18.5%, and on the average the error is about 11.3% and 15.7% for Eq. (14), together with Eq. (1), and for Eq. (25), respectively. Considering the various sources of error, the agreement of the analytical predictions with the empirical data is fairly good.

We further verified the models by comparing its predictions with the values of hardness measured by Tabor [11] on cylindrical specimens with known effective strain (Fig. 7). The predictions of the models agree quite well with the data.

In order to verify the proposed models, in addition to the hardness measurements of the previous researchers, we conducted cold extrusion experiments and measured Brinell hardness at the centerline of the extruded part.

In cold forming, usually low-carbon steels are used. Accordingly, the selected materials for extrusion were C40 and St37. Billets were normalized before the cold forming experiments in order to attain a homogenous and relatively soft microstructure. First, in order to characterize plastic flow behavior of the materials, i.e. to obtain the flow curve constants, upsetting experiments were carried out. Table 2 presents the constants of the flow curves represented by a power relation, $\sigma = \kappa\varepsilon^n$.

For extrusion tests, five extrusion ratios were chosen, which resulted in five different final strain values. Table 3 shows the dimensions of the extruded part, and the associated central strains. The details of the experimental procedure can be found in Refs. [60] and [61].

Although the effective strain at the centerline of the extruded part was analytically determined as $2\ln(D_0/D_e)$, due to edge effects validity of this formula is restricted to portions of cen-

Table 2
Flow curve constants of C40 and St37 ($\sigma = \kappa\varepsilon^n$)

Material	K (MPa)	n
C40	810	0.150
St37	773	0

Table 3
Strains and extrusion ratios of the extruded parts

Part number	Initial diameter, D_0 (mm)	Extruded diameter, D_e (mm)	True strain, $2\ln(D_0/D_e)$
1	30.2	15	1.40
2	27.3	15	1.20
3	23.5	15	0.90
4	19.3	15	0.50
5	17.0	15	0.25

Table 4
Average measured values of Brinell hardness at the centerline of the extruded parts and corresponding impression diameters

Strain	H_B (kgf/mm^2)		d (mm)	
	C40	St37	C40	St37
0.25	205	195	4.21	4.32
0.50	230	220	3.99	4.08
0.90	250	235	3.83	3.95
1.20	260	245	3.76	3.87
1.40	265	250	3.73	3.83

terline away from the edges. In order to investigate the range for which this formula is valid, the extrusion process was modeled using Marc Autoforge, and the effective strain distribution was determined. One may refer to Ref. [60] for the details of this analysis. After performing the FE simulations, the centerline strains were observed to be equal to the value $2\ln(D_0/D_e)$ away from the edges. Measurements were taken in the region where edge effects were not observed to make a valid comparison between the analytically predicted and measured values.

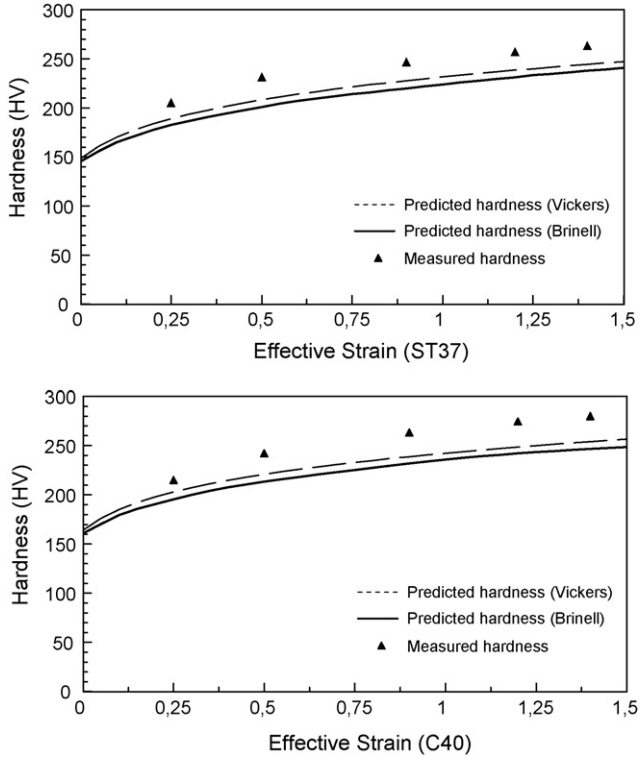

Fig. 8. Data points indicate the measured Brinell hardness (kgf/mm^2). The solid line and dashed line show the hardness predicted by Eq. (14), together with Eq. (1), and Eq. (25), respectively.

The extruded parts were cut at the mid-plane and the Brinell hardness measurements ($F/D^2 = 30$) were taken at the centerline of the extruded portion. Table 4 lists the average of the measured Brinell hardness (five measurements for each extruded specimen), and the corresponding impression diameter. These are the average values of 20 extruded specimens for each strain and material. 200 specimens were extruded totally.

The analytical models were then used to determine the hardness at the centerline. Fig. 8 gives a comparison between measured and predicted hardness. Again Brinell hardness is converted to Vickers hardness. Although the proposed equation underestimates the hardness, the predicted trend of the change in hardness with effective strain conforms well to the experimentally determined trend. The maximum error is less than 13%, which can be considered to be satisfactory for predicting hardness distribution in cold forged parts.

6. Discussion

Accuracy of the proposed equations is good considering that there may be numerous sources of error. As a source of measurement errors, piling-up or sinking-in around the circumference of the impression may detract from the accuracy of optical readings. Besides, we extensively used the conversion table between Vickers and Brinell hardness. Conversion factors have limited accuracy. The behavior of the material in resisting indentation could be different for spherical and pyramidal indenters. Also, any inhomogeneity may cause different readings especially for Vickers hardness, which has much smaller impression than Brinell's. On the other hand, large size of Brinell's impression leads to homogenization of mechanical properties. Especially, at locations where hardness gradient is high, Brinell hardness represents average hardness around the point at which measurement is taken. Impression size to part size ratio in our experiments as indicated in Table 4 is high, which might have led to overestimation in measured values. Besides, sometimes specimens were cut to take measurements in an interior region. During cutting operation, induced plastic deformation may increase the hardness.

The source of error may also lie in the model. Stress-strain curve of a material may not perfectly fit into a power relation as assumed in employing Eq. (4). Equality of *"m"* in Eq. (5) and "n" of Eq. (4) was assumed in the model. However, these exponents do not exactly have the same values. Also, the universality of α and β in Eq. (10), c and ε_e in Eq. (24) and their particular values used in this study were just approximations.

7. Conclusions

In this study, we presented analytical models to predict Brinell and Vickers hardness distribution in cold formed products. Application of these models require only flow curve constants (κ and n), which can be obtained through a simple compression test, and effective strain distribution, which can be obtained through

a FE analysis of the cold forming process. The predictions of the models were compared with experimental data, and the accuracy of these predictions was quite satisfactory.

Acknowledgments

This paper is based on the work supported by KANCA, a cold forging company, and the Scientific Research Projects of Bogazici University with the code number 04A602.

References

[1] H. Kim, S.-M. Lee, T. Altan, Prediction of hardness distribution in cold backward extruded cups, J. Mater. Process. Technol. 59 (1996) 113–121.
[2] B.P.P.A. Gouveia, J.M.C. Rodrigues, P.A.F. Martins, Steady state finite-element analysis of cold forward extrusion, J. Mater. Process. Technol. 73 (1998) 281–288.
[3] B.P.P.A. Gouveia, J.M.C. Rodrigues, P.A.F. Martins, Finite element modeling of cold forward extrusion and combined Eulerian–Lagrangian formulations, J. Mater. Process. Technol. 80–81 (1998) 647–652.
[4] J. Petruska, L. Janicek, On the evaluation of strain inhomogeneity by hardness measurement of formed products, J. Mater. Process. Technol. 143–144 (2003) 300–305.
[5] M. Ruminski, J. Luksza, J. Kusiak, M. Packo, Analysis of the effect of die shape on the distribution of mechanical properties and strain field in the tube sinking process, J. Mater. Process. Technol. 80–81 (1998) 683–689.
[6] Y. Choi, J.H. Park, B.M. Kim, J.C. Choi, B.H. Min, Estimation of relation between effective strain and hardness by rigid-plastic FEM, Met. Mater. 6 (2) (2000) 111–116.
[7] A.E. Tekkaya, Improved relationship between Vickers hardness and yield stress for cold formed materials, Steel Res. 72 (8) (2001) 304–310.
[8] H.E. Boyer, Hardness Testing, ASM International, USA, 1987.
[9] D. Tabor, The Hardness of Metals, Clarendon Press, New York, 1951.
[10] D. Tabor, Indentation hardness: fifty years on, a personal view, Philos. Mag. A 74 (5) (1996) 1207–1212.
[11] D. Tabor, A simple theory of static and dynamic hardness, Proc. R. Soc. Lond. Ser.A, Math. Phys. Sci. 192 (1029) (1948) 247–274.
[12] Y. Tirupataiah, G. Sundararajan, On the constraint factor associated with the indentation of work-hardening materials with a spherical ball, Metall. Trans. A 22 (1991) 2375–2384.
[13] M.M. Chaudhri, Subsurface plastic strain distribution around spherical indentations in metals, Philos. Mag. A 74 (5) (1996) 1213–1224.
[14] S. Timoshenko, J.N. Goodier, Theory of Elasticity, McGraw-Hill, 1951.
[15] G.B. Sinclair, P.S. Follansbee, K.L. Johnson, Quasi-static normal indentation of an elasto-plastic half space by a rigid sphere-II results, Int. J. Solids Struct. 21 (8) (1985) 865–888.
[16] H.A. Francis, Phenomenological analysis of plastic spherical indentation, Trans. ASME; J. Eng. Mater. Technol. 98 (1976) 272–281.
[17] W.F. Chen, D.J. Han, Plasticity for Structural Engineers, Springer–Verlag, New York, 1988.
[18] A.P. Singh, K.A. Padmanabhan, G.N. Pandey, G.M.D. Murty, S. Jha, Strength differential effect in four commercial steels, J. Mater. Sci. 35 (2000) 1379–1388.
[19] O. Richmond, H.L. Morrison, M.L. Devenpeck, Sphere indentation with application to the Brinell hardness test, Int. J. Mech. Sci. 16 (1974) 75–82.
[20] S. Biwa, B. Storakers, An analysis of fully plastic Brinell indentation, J. Mech. Phys. Solids 43 (8) (1995) 1303–1333.
[21] J.R. Matthews, Indentation hardness and hot pressing, Acta Metall. 28 (1980) 311–318.
[22] P.S. Follansbee, G.B. Sinclair, Quasi-static normal indentation of an elasto-plastic half-space by a rigid sphere-I. Analysis, Int. J. Solids Struct. 20 (1984) 81–91.
[23] M.L. Edlinger, P. Gratacos, P. Montmitonnet, E. Felder, Finite element analysis of elastoplastic indentation with a deformable indenter, Eur. J. Mech. A/Solids 12 (5) (1993) 679–698.
[24] N. Guyot, F. Kosior, G. Maurice, Numerical study of the Brinell hardness test of elastoplastic indentation, ZAMM Z. Angew. Math. Mech. 80 (8) (2000) 555–563.
[25] R. Hill, B. Storakers, A.B. Zdunek, A theoretical study of the Brinell hardness test, Proc. R. Soc. Lond. A 423 (1989) 301–330.
[26] S. Mesarovic, N.A. Fleck, Spherical indentation of elastic–plastic solids, Proc. R. Soc. Lond. 455 (1999) 2707–2728.
[27] M.M. Chaudri, Strain hardening around spherical indentations, Phys. Status Solidi (a) 182 (2) (2000) 641–652.
[28] B. Taljat, T. Zacharia, F. Kosel, New analytical procedure to determine stress–strain curve from spherical indentation data, Int. J. Solids Struct. 35 (33) (1998) 4411–4426.
[29] Y. Tirupataiah, G. Sundararajan, A comprehensive analysis of the static indentation process, Mater. Sci. Eng. 91 (1987) 169–180.
[30] J.-H. Ahn, D. Kwon, Derivation of plastic–stress relationship from ball indentations: examination of strain definition and pileup effect, J. Mater. Res. 16 (11) (2001) 3170–3178.
[31] P.-L. Larsson, Investigation of sharp contact at rigid-plastic conditions, Int. J. Mech. Sci. 43 (2001) 895–920.
[32] S. Jayaraman, G.T. Hahn, W.C. Oliver, C.A. Rubin, Determination of monotonic stress–strain curve of hard materials from ultra-low-load indentation tests, Int. J. Solids Struct. 35 (5–6) (1998) 365–381.
[33] K.L. Johnson, The correlation of indentation experiments, J. Mech. Phys. Solids 18 (1970) 115–126.
[34] D.M. Marsh, Plastic flow in glass, Proc. R. Soc. Lond. A 279 (1964) 420–435.
[35] R. Hill, The Mathematical Theory of Elasticity, Clarendon Press, Oxford, 1950.
[36] C.J. Studman, M.A. Moore, S.E. Jones, On the correlation of indentation experiments, J. Phys. D: Appl. Phys. 10 (1977) 949–956.
[37] A.E. Giannakopoulos, P.-L. Larsson, R. Vestergaard, Analysis of Vickers indentation, Int. J. Solids Struct. 31 (19) (1994) 2679–2708.
[38] M. Mata, M. Anglada, J. Alcala, A hardness equation for sharp indentation of elastic-power-law strain-hardening materials, Philos. Mag. A 82 (10) (2002) 1831–1839.
[39] M. Mata, J. Alcala, Mechanical property evaluation through sharp indentations in elastoplastic and fully plastic contact regimes, J. Mater. Res. 18 (7) (2003) 1705–1709.
[40] M. Mata, J. Alcala, The role of friction on sharp indentation, J. Mech. Phys. Solids 52 (2004) 145–165.
[41] Y.-T. Cheng, Z. Li, Hardness obtained from conical indentations with various cone angles, J. Mater. Res. 15 (12) (2000) 2830–2835.
[42] Y.-T. Cheng, C.-M. Cheng, What is indentation hardness? Surf. Coat. Technol. 133–134 (2000) 417–424.
[43] Y.-T. Cheng, C.-M. Cheng, Scaling, dimensional analysis, and indentation measurements, Mater. Sci. Eng. R 44 (2004) 91–149.
[44] Z. Li, Y.-T. Cheng, H.T. Yang, S. Chandrasekar, On two indentation hardness definitions, Surf. Coat. Technol. 154 (2002) 124–130.
[45] A. Bolshakov, G.M. Pharr, Influences of pileup on the measurement of mechanical properties by load and depth sensing indentation techniques, J. Mater. Res. 13 (4) (1998) 1049–1058.
[46] M. Dao, N. Chollacoop, K.J. Van Vliet, T.A. Venkatesh, S. Suresh, Computational modeling of the forward and reverse problems in instrumented sharp indentation, Acta Mater. 49 (2001) 3899–3918.
[47] N. Chollacoop, M. Dao, S. Suresh, Depth—sensing instrumented indentation with dual sharp indenters, Acta Mater. 51 (2003) 3713–3729.
[48] J.L. Bucaille, S. Stauss, E. Felder, J. Michler, Determination of plastic properties of metals by instrumented indentation using different sharp indenters, Acta Mater. 51 (2003) 1663–1678.
[49] O. Casals, J. Alcala, The duality in mechanical property extractions from Vickers and Berkovich instrumented indentation experiments, Acta Mater. 53 (2005) 3545–3561.
[50] D.R. Kumar, Formability analysis of extra-deep drawing steel, J. Mater. Process. Technol. 130–131 (2002) 31–41, and personal communication.
[51] A. Nayebi, R. El Abdi, O. Bartier, G. Mauvoisin, New procedure to determine steel mechanical properties from the spherical indentation technique, Mech. Mater. 34 (2002) 243–254.

[52] Y. Murakami, K. Matsuda, Analysis of Vickers hardness by finite element method, Trans. ASME; J. Appl. Mech. 61 (1994) 822–828.
[53] K.M. Rajan, P.U. Deshpande, K. Narasimhan, Effect of heat treatment of preform on the mechanical properties of flow formed AISI 4130 steel tubes—a theoretical and experimental assessment, J. Mater. Process. Technol. 125–126 (2002) 503–511.
[54] J. Alcala, A.C. Barone, M. Anglada, The influence of plastic hardening on surface deformation modes around Vickers and spherical indents, Acta Mater. 48 (2000) 3451–3464.
[55] N.E. Dowling, Mechanical Behavior of Materials: Engineering Methods for Deformation Fracture and Fatigue, Prentice Hall, NJ, 1999.
[56] S. Carlsson, P.-L. Larsson, On the determination of residual stress and strain fields by sharp indentation testing. Part II. Experimental investigation, Acta Mater. 49 (2001) 2193–2203.
[57] M.T. Milan, D. Spinelli, W.W. Bose Filho, M.F.V. Montezuma, V. Tita, Failure analysis of a SAE 4340 steel locking bolt, Eng. Fail. Anal. 11 (6) (2004) 915–924.
[58] K. Matsuda, Prediction of stress–strain curves of elastic–plastic materials based on Vickers indentation, Philos. Mag. A 82 (10) (2002) 1941–1951.
[59] E. Oberg, F.D. Jones, H.L. Horton, Machinery's Handbook, 21st ed., Industrial Press Inc., New York, 1979.
[60] A. Demir, 2001. Prediction of Brinell hardness distribution in cold formed parts, MS thesis, Bogazici University, Istanbul.
[61] A. Demir, F.O. Sonmez, Prediction of Brinell hardness distribution in cold formed parts, Trans. ASME; J. Eng. Mater. Technol. 126 (2004) 398–405.